


RESEARCH ARTICLE

The Lid/KDM5 histone demethylase complex activates a critical effector of the oocyte-to-zygote transition

Daniela Torres-Campana¹ , Shuhei Kimura² , Guillermo A. Orsi¹ , Béatrice Horard¹, Gérard Benoit¹ , Benjamin Loppin^{1*} 

1 Laboratoire de Biologie et de Modélisation de la Cellule, CNRS UMR5239, Ecole Normale Supérieure de Lyon, University of Lyon, France, **2** Laboratoire de Biométrie et Biologie Evolutive, Université Lyon 1, CNRS, UMR 5558, Villeurbanne F-69622, France

 These authors contributed equally to this work.

 Current address: Seto Hospital, Kanayama-cho, Tokorozawa-shi, Saitama-ken, Japan

* benjamin.loppin@ens-lyon.fr



 OPEN ACCESS

Citation: Torres-Campana D, Kimura S, Orsi GA, Horard B, Benoit G, Loppin B (2020) The Lid/KDM5 histone demethylase complex activates a critical effector of the oocyte-to-zygote transition. *PLoS Genet* 16(3): e1008543. <https://doi.org/10.1371/journal.pgen.1008543>

Editor: Giovanni Bosco, Geisel School of Medicine at Dartmouth, UNITED STATES

Received: June 28, 2019

Accepted: November 26, 2019

Published: March 5, 2020

Copyright: © 2020 Torres-Campana et al. This is an open access article distributed under the terms of the [Creative Commons Attribution License](https://creativecommons.org/licenses/by/4.0/), which permits unrestricted use, distribution, and reproduction in any medium, provided the original author and source are credited.

Data Availability Statement: The DNA sequencing data from this publication have been deposited to the Gene Expression Omnibus database [<https://www.ncbi.nlm.nih.gov/geo/>] and assigned the identifier GSE133064 (RNA-Seq) and GSE133202 (ChIP-Seq).

Funding: SK was supported by a fellowship from the Agence Nationale de la Recherche (<https://anr.fr>) (ZygoPat ANR-12-BSV6-0014). The funders had no role in study design, data collection and

Abstract

Following fertilization of a mature oocyte, the formation of a diploid zygote involves a series of coordinated cellular events that ends with the first embryonic mitosis. In animals, this complex developmental transition is almost entirely controlled by maternal gene products. How such a crucial transcriptional program is established during oogenesis remains poorly understood. Here, we have performed an shRNA-based genetic screen in *Drosophila* to identify genes required to form a diploid zygote. We found that the Lid/KDM5 histone demethylase and its partner, the Sin3A-HDAC1 deacetylase complex, are necessary for sperm nuclear decompaction and karyogamy. Surprisingly, transcriptomic analyses revealed that these histone modifiers are required for the massive transcriptional activation of *deadhead* (*dhd*), which encodes a maternal thioredoxin involved in sperm chromatin remodeling. Unexpectedly, while *lid* knock-down tends to slightly favor the accumulation of its target, H3K4me3, on the genome, this mark was lost at the *dhd* locus. We propose that Lid/KDM5 and Sin3A cooperate to establish a local chromatin environment facilitating the unusually high expression of *dhd*, a key effector of the oocyte-to-zygote transition.

Author summary

Nuclear enzymes that add or remove epigenetic marks on histone tails potentially control gene expression by affecting chromatin structure and DNA accessibility. For instance, members of the KDM5 family of histone demethylases specifically remove methyl groups on the lysine 4 of histone H3, a mark generally correlated with gene expression. Lid (Little imaginal discs), the *Drosophila* KDM5, is essential for viability but is also required for female fertility. In this paper, we have found that the specific removal of Lid in developing oocytes perturbs the decompaction of the sperm nucleus at fertilization and the integration of paternal chromosomes in the zygote. Sperm nuclear decompaction normally requires the presence of a small redox protein called Deadhead (Dhd), which is massively

analysis, decision to publish, or preparation of the manuscript.

Competing interests: The authors have declared that no competing interests exist.

expressed at the end of oogenesis. Strikingly, our analyses of ovarian transcriptomes revealed that the absence of Lid completely abolishes the expression of *dhd*. This direct functional link between a general histone modifier and the expression of an essential terminal effector gene represents a rare finding. We hope that our work will help understanding how histone demethylases function in controlling complex developmental transitions as well as cancer progression.

Introduction

In sexually reproducing animals, fertilization allows the formation of a diploid zygote through the association of two haploid gametes of highly different origins and structures. Generally, the spermatozoon delivers its compact nucleus within the egg cytoplasm, along with a pair of centrioles, while the egg provides one haploid meiotic product and all resources to sustain zygote formation [1]. In some species, this maternal control extends to early embryo development, as in *Drosophila melanogaster*, where the initial amplification of embryo cleavage nuclei occurs without significant zygotic transcription [2]. Instead, the bulk of transcriptional activity takes place in the fifteen interconnected large polyploid germline nurse cells that deposit gene products in the cytoplasm of the growing oocyte [3]. The developmental potential of the egg is thus initially dependent on the establishment of a highly complex transcriptional program in female germ cells.

One of the earliest events of the oocyte-to-zygote transition is the rapid transformation of the fertilizing sperm nucleus into a functional male pronucleus. In *Drosophila*, the needle-shaped, highly compact sperm nucleus is indeed almost entirely organized with non-histone, Sperm Nuclear Basic Proteins (SNBPs) of the protamine-like type [4,5]. Male pronucleus formation begins with the genome-wide replacement of SNBPs with maternally supplied histones, a process called sperm chromatin remodeling, which is followed by extensive pronuclear decondensation [1]. Finally, zygote formation involves the coordinated migration and apposition of male and female pronuclei and the switch from meiotic to mitotic division within the same cytoplasm.

Here, we report the results of a genetic screen specifically designed to find new genes required for the oocyte-to-zygote transition in *Drosophila*. Our screen identified two histone modifiers, the Lid/KDM5 histone H3K4me3 demethylase and the Sin3A-HDAC1 histone deacetylase complex, which are both required for the integration of paternal chromosomes into the zygote. These interacting epigenetic factors are known to regulate the expression of hundreds of genes in somatic tissues but their role in the establishment of the ovarian transcriptome is unknown. Strikingly, RNA-Sequencing analyses revealed that, despite the modest impact of their depletion on ovarian transcripts, Lid and Sin3A are critically required for the massive expression of *deadhead* (*dhd*), a key effector of the oocyte-to-zygote transition [6,7]. Furthermore, we demonstrate that germline knock-down of these histone modifiers specifically prevent sperm chromatin remodeling through a mechanism that depends on the DHD thioredoxin.

Results & discussion

A maternal germline genetic screen for gynohaploid embryo development

We performed an *in vivo* RNA interference screen in the female germline to identify genes required for the integration of paternal chromosomes in the zygote. In *Drosophila*, failure to

form a male pronucleus following fertilization is generally associated with the development of haploid embryos that possess only maternally-derived chromosomes (gynohaploid embryos) and that never hatch [8]. We chose to screen transgenic lines from the TRiP collection that express small hairpin RNAs (shRNAs) under the control of the Gal4 activator [9]. We selected shRNA lines that targeted genes with known or predicted chromatin-related function and that show adult ovarian expression (Flybase). Among the 374 tested TRiP lines, 157 (41.9%) induced female sterility or severely reduced fertility when induced with the germline-specific *P*{*GAL4::VP16-nos.UTR*}^{MVDI} Gal4 driver (*nos*-Gal4), thus underlying the importance of chromatin regulation for oogenesis and early embryo development (S1 Table). We then specifically searched for shRNAs that induced a maternal effect embryonic lethal phenotype associated with gynohaploid development (Fig 1A). Gynohaploid embryos can be efficiently identified by scoring the zygotic expression of a paternally-transmitted *P*[*g-GFP::cid*] transgene at the gastrulation stage or beyond [10]. Among the sterile lines with late developing embryos (class 4 in Fig 1A and S1 Table) that were identified, four shRNA lines (GLV21071, GL00612, HMS00359 and HMS00607) produced embryos that were negative for GFP::CID (Fig 1B). Note that none of these shRNAs induced complete female sterility and about 1 to 4% of embryos hatched and were thus diploid (Table 1).

Two of the identified lines (GLV21071 and GL00612) express the same shRNA against the *little imaginal disc* (*lid*) gene, which encodes the single fly member of the KDM5/JARID1A family of histone demethylases [11,12]. KDM5 demethylases specifically target the trimethylation of lysine 4 of histone H3 (H3K4me3), a mark typically enriched around the Transcriptional Start Site (TSS) of transcriptionally active genes [13,14]. The two other shRNAs (HMS00359 and HMS00607) target the *Sin3A* and *HDAC1/rpd3* genes, respectively. The conserved Sin3A protein scaffold interacts with the histone lysine deacetylase HDAC1 to form the core SIN3 histone deacetylase complex, which is generally considered as a transcriptional repressor [15]. The SIN3 complex regulates the expression of genes involved in a number of metabolic and developmental processes [16–19]. Interestingly, Lid and the largest Sin3A isoform were previously shown to physically and functionally interact [16,17,20,21], thus opening the possibility that these histone modifiers could control the same pathway leading to the formation of a diploid zygote.

Lid and SIN3 are required for sperm chromatin remodeling at fertilization

The Lid demethylase has been previously shown to be required in the female germline for embryo viability [22,23]. Both studies reported a dual phenotype for eggs produced by *lid* KD females (hereafter called *lid* KD eggs): while a majority of eggs fail to initiate development, a variable but significant fraction developed but died at later stages. Our own observations confirmed that about 15% of *lid* KD embryos reach or develop beyond the blastoderm stage (S1 Fig). Furthermore, our analysis of *P*[*g-GFP::cid*] expression (Fig 1B) indicates that most of these late, non viable KD embryos are haploid and develop with maternal chromosomes. To follow the fate of paternal chromosomes in *lid* KD eggs, we crossed *lid* KD females with males expressing the sperm chromatin marker Mst35Ba::GFP (ProtA::GFP) [24]. In *Drosophila*, protamine-like proteins such as Mst35Ba are rapidly removed from sperm chromatin at fertilization [1] and, accordingly, ProtA::GFP is never observed in the male nucleus of control eggs. In striking contrast, the vast majority of fertilized *lid* KD eggs contained a needle-shaped sperm nucleus that was still positive for ProtA::GFP, indicating that sperm chromatin remodeling was compromised (Fig 1C and 1D). Anti-histone immunostaining indeed revealed that the replacement of SNBPs with maternally supplied histones was variable in KD eggs, ranging from complete absence of histones in the sperm nucleus to the coexistence of variable amounts

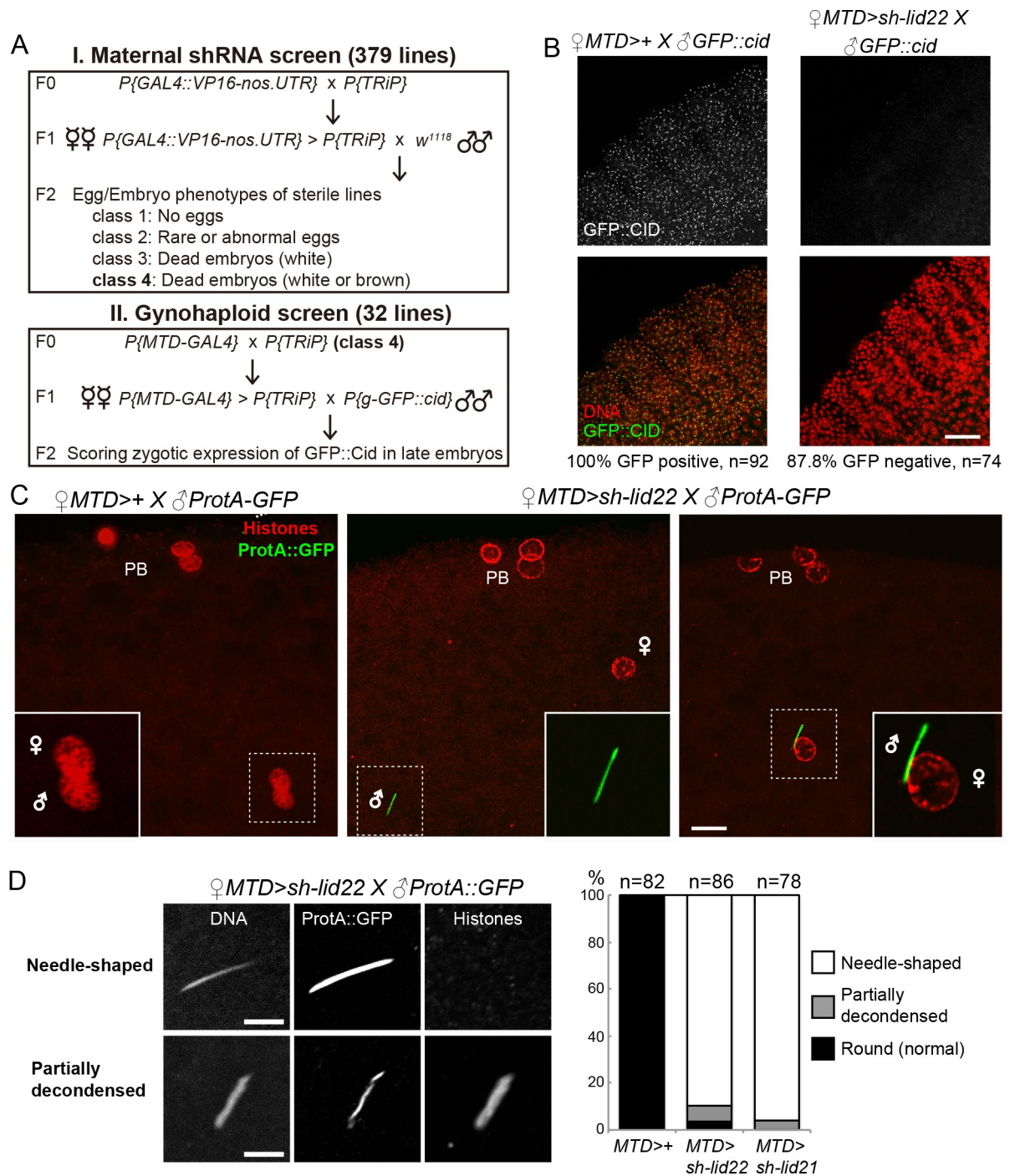


Fig 1. Lid is required for sperm nuclear decompaction at fertilization. A—Scheme of shRNA screen in the female germline. B—Left: Zygotic expression of a paternally-derived $P[g-GFP::cid]$ transgene in a control embryo. GFP::Cid marks centromeric chromatin and is visible as nuclear dots. Right: *lid* KD females produce embryos that fail to express the paternally-inherited transgene. Scale bar: 25 μ m. C—Maternal Lid is required for SNBP removal and sperm nuclear decompaction at fertilization. Left: a control egg at pronuclear apposition. Both pronuclei (inset) appear similar in size and shape and the SNBP marker ProtA::GFP is not detected. Middle: A representative *lid* KD egg containing a needle-shaped sperm nucleus (inset) still packaged with ProtA::GFP. Right: A fertilized *lid* KD egg with the sperm nucleus apposed to the female pronucleus. Scale bar: 10 μ m. D—SNBP replacement with histones is impaired in *lid* KD eggs. Left: Confocal images of representative sperm nuclei in *lid* KD eggs. Partially decondensed nuclei are positive for histones. Scale bar: 5 μ m. Right: Quantification of sperm nuclear phenotype in control and *lid* KD eggs.

<https://doi.org/10.1371/journal.pgen.1008543.g001>

Table 1. Embryo hatching rates.

Female genotype	Male genotype	Number of eggs	Hatch. rate (%)
<i>w</i> ¹¹¹⁸	<i>w</i> ¹¹¹⁸	344	97.67
<i>dhd</i> ^{Δ5}	<i>w</i> ¹¹¹⁸	375	0.00
<i>dhd</i> ^{Δ5} / <i>FM7c</i>	<i>w</i> ¹¹¹⁸	573	78.36
<i>MTD</i> >+	<i>w</i> ¹¹¹⁸	1561	98.27
<i>MTD</i> > <i>sh-lid22</i>	<i>w</i> ¹¹¹⁸	1403	2.14
<i>MTD</i> > <i>sh-lid21</i>	<i>w</i> ¹¹¹⁸	1144	1.05
<i>MTD</i> > <i>sh-Sin3A</i>	<i>w</i> ¹¹¹⁸	1221	0.25
<i>MTD</i> > <i>sh-rpd3</i>	<i>w</i> ¹¹¹⁸	521	4.03
<i>MTD</i> > <i>sh-Hira</i>	<i>w</i> ¹¹¹⁸	315	0.00
Rescue with <i>P[dhd</i>^{WT}] genomic transgene			
<i>dhd</i> ^{Δ5} ; <i>P[dhd]</i>	<i>w</i> ¹¹¹⁸	663	85.67
<i>dhd</i> ^{Δ5} ; <i>P[dhd]</i> / <i>TM2</i>	<i>w</i> ¹¹¹⁸	884	94.57
<i>MTD</i> > <i>sh-lid22</i> , <i>P[dhd]</i>	<i>w</i> ¹¹¹⁸	1159	4.57
Rescue with <i>P[gnu-dhd</i>^{WT}] transgene			
<i>dhd</i> ^{Δ5} ; <i>P[gnu-dhd]</i>	<i>w</i> ¹¹¹⁸	331	7.25
<i>dhd</i> ^{Δ5} ; <i>P[gnu-dhd]</i> / <i>TM2</i>	<i>w</i> ¹¹¹⁸	1059	3.40
<i>MTD</i> > <i>sh-lid22</i> , <i>P[gnu-dhd]</i> /+	<i>w</i> ¹¹¹⁸	695	7.48
Rescue with <i>P[UASP-dhd]</i> inducible transgenes			
<i>nos</i> >+	<i>w</i> ¹¹¹⁸	711	95.36
<i>nos</i> > <i>P[UASP-dhd]</i> /+	<i>w</i> ¹¹¹⁸	450	97.33
<i>dhd</i> ^{Δ5} ; <i>nos</i> > <i>P[UASP-dhd]</i>	<i>w</i> ¹¹¹⁸	1163	90.28
<i>dhd</i> ^{Δ5} ; <i>nos</i> > <i>P[UASP-dhd</i> ^{SXXS}]	<i>w</i> ¹¹¹⁸	702	0.00
<i>MTD</i> > <i>sh-lid22</i> , <i>P[UASP-dhd]</i>	<i>w</i> ¹¹¹⁸	1343	28.44
<i>MTD</i> > <i>sh-lid22</i> , <i>P[UASP-dhd</i> ^{SXXS}]	<i>w</i> ¹¹¹⁸	315	14.60
<i>nos</i> > <i>sh-lid21</i>	<i>w</i> ¹¹¹⁸	1508	1.92
<i>nos</i> > <i>P[UASP-dhd]</i> / <i>sh-lid21</i>	<i>w</i> ¹¹¹⁸	383	19.32
<i>nos</i> > <i>sh-Sin3a</i>	<i>w</i> ¹¹¹⁸	542	2.03
<i>nos</i> > <i>P[UASP-dhd]</i> / <i>sh-Sin3a</i>	<i>w</i> ¹¹¹⁸	621	8.86
<i>nos</i> > <i>sh-Rpd3</i>	<i>w</i> ¹¹¹⁸	919	2.94
<i>nos</i> > <i>P[UASP-dhd]</i> / <i>sh-Rpd3</i>	<i>w</i> ¹¹¹⁸	395	7.59
<i>nos</i> > <i>sh-Hira</i>	<i>w</i> ¹¹¹⁸	514	0.00
<i>nos</i> > <i>P[UASP-dhd]</i> / <i>sh-Hira</i>	<i>w</i> ¹¹¹⁸	380	0.00

<https://doi.org/10.1371/journal.pgen.1008543.t001>

of histones and ProtA::GFP (Fig 1D). Notably, we noticed that partially decondensed sperm nuclei in *lid* KD eggs were systematically positive for histones. Taken together, our observations indicate that sperm chromatin remodeling is severely impaired in *lid* KD eggs, thus explaining the absence of paternal chromosomes in most developing embryos.

Germline depletion of Lid was previously shown to affect karyosome morphology and chromosome positioning in metaphase I oocytes [25]. In contrast, another study had previously reported that meiotic progression was not affected in *lid* KD oocytes [22]. Interestingly, although our own observations indeed confirmed the aberrant karyosome structure in *lid* KD oocytes, we observed that the second meiotic division appeared to resume normally in a vast majority of *lid* KD eggs (S2 Fig). We noted, however, that, following meiosis, the female pronucleus frequently (62%, n = 76) failed to appose to the sperm nucleus in *lid* KD eggs (Fig 1C). Thus, we propose that defective pronuclear migration largely accounts for the previously reported failure of *lid* KD embryos to initiate cleavage divisions [23]. Like Navarro-Costa

et al., we noted that the rosette of polar body chromosomes was frequently abnormal in morphology, but this phenotype appeared independent of meiosis *per se*.

Remarkably, we found that germline KD of *Sin3A* also induced a highly penetrant sperm nuclear phenotype with all scored fertilizing sperm nuclei retaining a needle-like shape (100%, $n = 19$) (S3 Fig). Finally, a similar but less penetrant phenotype was also observed in *rpd3* KD eggs (S3 Fig). As this low penetrance could result from less efficient gene knock-down, we chose to mainly focus on *lid* and *Sin3A* in the rest of this study.

Transcriptomic analysis of *lid* KD and *Sin3A* KD ovaries identifies *deadhead* as a common and major target gene

In eggs from wild-type females, anti-Lid immunostaining failed to detect Lid protein in the male or female pronucleus, thus suggesting that its implication in sperm chromatin remodeling was indirect. In fact, Lid was not detected in embryos before the blastoderm stage (S4 Fig). We thus turned to RNA sequencing (RNA Seq) to analyze the respective impact of *lid* KD and *Sin3A* KD on the ovarian transcriptome.

We compared transcriptomes obtained from *lid* KD or *Sin3A* KD ovaries (using the maternal triple driver MTD-Gal4) with control transcriptomes (MTD-Gal4 only). Globally, our analyses revealed a relatively modest impact of *lid* KD and *Sin3A* KD on ovarian gene expression, with more genes downregulated in both cases (Fig 2B and S5 Fig; S2 Table). Note that these changes are expected to reflect the activity of Lid and Sin3A in germ cells, as ovarian somatic cells (see Fig 2A) do not express the targeting shRNAs. In their transcriptome analysis (based on microarrays) of *lid* KD wing imaginal discs, Azorin and colleagues found a similar number of differentially-expressed genes, most of them being downregulated [14]. However, RNA Seq analyses recently published by Drelon *et al.* in contrast found 1630 genes (FDR<0.05) dysregulated in wing discs from a null *lid* mutant [26]. Moreover, Liu and Secombe [27] found 8,056 genes differentially expressed (60% were down-regulated) in *lid* adult mutant flies (FDR<0.05), a number which could reflect the greater cell type complexity involved in this analysis.

We found that only 29% (139) of the 473 differentially-expressed genes in *lid* KD were also differentially-expressed in *Sin3A* KD, and only 100 genes (21%) were dysregulated in the same direction in both KD (Fig 2B). As a matter of comparison, Gajan *et al.* found a 65% overlap in *Drosophila* S2 cells [17]. As the *Sin3A* shRNA that we used targets all predicted alternatively spliced mRNAs, this suggests that the knock-down affects Sin3A isoforms with Lid-independent functions [16].

Remarkably, however, we noticed that the *deadhead* (*dhd*) gene was by far the most severely impacted gene, downregulated by more than two orders of magnitude in both *lid* KD and *Sin3A* KD transcriptomes (Fig 2C, S6 Fig). The implication of *dhd* appeared particularly interesting because we and others have recently established that this germline-specific gene is critically required for sperm nuclear decompaction at fertilization [6,28]. *dhd* indeed encodes a specialized thioredoxin that cleaves disulfide bonds on SNBPs, thus facilitating their removal from sperm chromatin [6,28]. RT-PCR and Western-blot analyses confirmed the severe down-regulation of *dhd* in *lid* KD and *Sin3A* KD (S5 Fig).

dhd is a small, intronless gene located in the middle of a cluster of fifteen densely packed genes spanning about 40 kb of genomic DNA. Interestingly, the *dhd* gene lies within a 1.4 kb region that is immediately flanked by two genes with testis-specific expression (*Trx-T* and *CG4198*) (Fig 2D). Despite this apparently unfavorable genomic environment, *dhd* is one of the most highly-expressed genes in ovaries [29], as confirmed by our RNA Seq profiles (Fig 2C and S6 Fig). Interestingly, although this 40 kb region contains six additional genes expressed

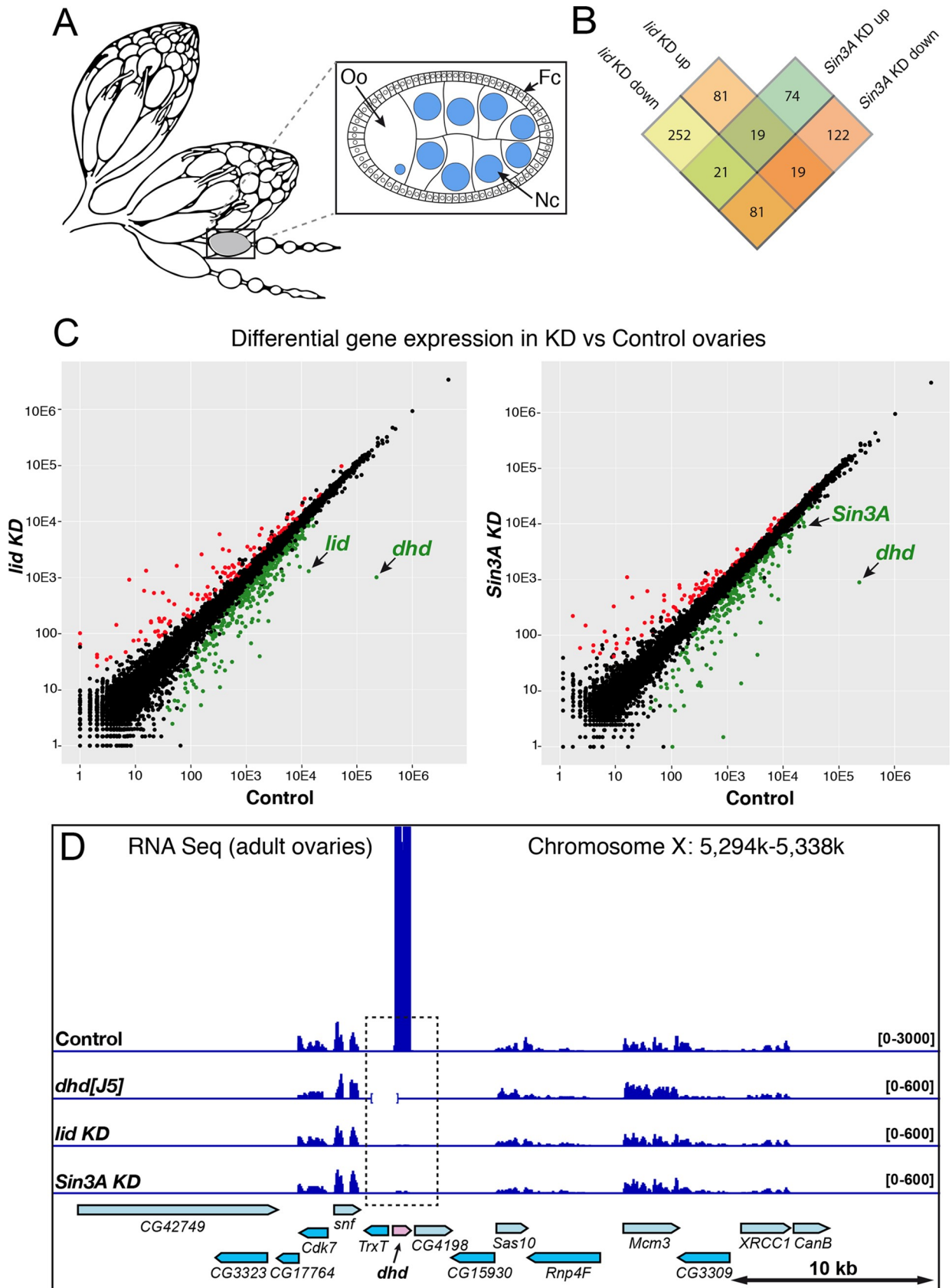


Fig 2. *deadhead* is strongly downregulated in *lid* KD and *Sin3A* KD ovaries. A—Scheme of a pair of adult ovaries with two isolated ovarioles and an egg chamber (inset). Germline nuclei are in blue. Oo: Oocyte, Nc: Nurse cells, Fc: Follicle cells. B—Venn diagram showing the number of differentially expressed genes in *lid* KD and *Sin3A* KD ovarian transcriptomes (FDR<0.001). C—Comparison of RNA seq normalized reads per gene (DESeq2) are shown for *lid* KD vs Control (left) and *Sin3A* KD vs Control (right). Genes with a negative foldchange (downregulated in KD) are in green (FDR<0.001). Genes with a positive foldchange (upregulated in KD) are in red (FDR<0.001). D—Integrative Genomics Viewer (igv) view of Control, *dhd*^[15], *lid* KD and *Sin3A* KD ovarian RNA Seq signal on the *dhd* region. The *Df(1)J5* deficiency is indicated as an interrupted baseline on the *dhd*^[15] track.

<https://doi.org/10.1371/journal.pgen.1008543.g002>

in ovaries, *dhd* is the only one affected by *lid* KD or *Sin3A* KD (Fig 2D). Thus, Lid and the SIN3 complex exert a critical and surprisingly specific control on the transcriptional activation of *dhd* in female germ cells.

Impact of Lid depletion on the distribution of H3K4me3 in ovaries

To evaluate the impact of *lid* KD on the distribution of its target histone mark in the female germline, we performed chromatin immunoprecipitation and sequencing (ChIP-Seq) analyses of H3K4me3 in ovaries from control and *lid* KD females. Consistent with earlier reports of a global increase of H3K4me3 in *lid* mutant tissues [14,23,25,30], we observed that H3K4me3 ChIP peaks in *lid* KD ovaries were globally more pronounced compared to control ovaries (Fig 3A). Our analysis actually revealed that about 10% (1528) of H3K4me3 identified peaks in control ovaries were significantly increased in *lid* KD ovaries (S3 Table; FDR<0.05). For those peaks that were associated with genes, the relative enrichment of H3K4me3 in *lid* KD ovaries mainly affected the promoter region and gene body (Fig 3B). A similar effect was previously observed in *lid* depleted wing imaginal discs, with H3K4me3 abundance specifically increased at the TSS of Lid direct target genes [14]. We nevertheless found 46 H3K4me3 peaks that were significantly decreased in *lid* KD ovaries compared to control ovaries (S3 Table; FDR<0.05). Among these, the H3K4me3 peak on the *dhd* gene was the second most severely affected (S3 Table and Fig 3C). Furthermore, only ten of the negatively affected peaks covered genes that were downregulated in *lid* KD ovaries, including *dhd*. Remarkably, the prominent H3K4me3 peak on *dhd* was almost completely lost in *lid* KD ovaries while other peaks within the *dhd* region remained essentially unchanged. *CG4198*, which lies immediately downstream of *dhd* is a notable exception, as this gene also shows a decrease of H3K4me3 (Fig 3C). In this case, however, it is interesting to note that the presence of the mark is not correlated with transcriptional activity.

At first, the paradoxical loss of H3K4me3 enrichment on the *dhd* gene upon Lid depletion suggests that the demethylase activity of Lid is not locally responsible for this regulation. In fact, it has been established that *lid* mutant females with a catalytic dead JmjC* *lid* rescue transgene are viable and at least partially fertile [23,26,31], thus suggesting that the catalytic activity of Lid is not absolutely required to form a viable zygote. To directly test the implication of the Lid demethylase domain in *dhd* regulation, we measured *dhd* expression in JmjC* rescued females. Surprisingly, *dhd* transcripts were severely reduced in these females compared to control females rescued with a wild-type *lid* transgene (S7 Fig). We thus conclude that the demethylase activity of Lid is important for *dhd* expression. At least two hypotheses could reconcile this conclusion with our ChIP-Seq results. First, it is possible that the demethylase activity of Lid is only transiently required at the *dhd* locus, perhaps to switch on its transcription at mid-oogenesis, while later, massive *dhd* expression would no longer require this activity. Alternatively, Lid could exert a control on *dhd* transcription by restricting the level of H3K4me3 at an enhancer element, similarly to what was previously reported for KDM5 demethylases in different model organisms [32–34]. Although our ChIP-Seq analyses failed to identify any

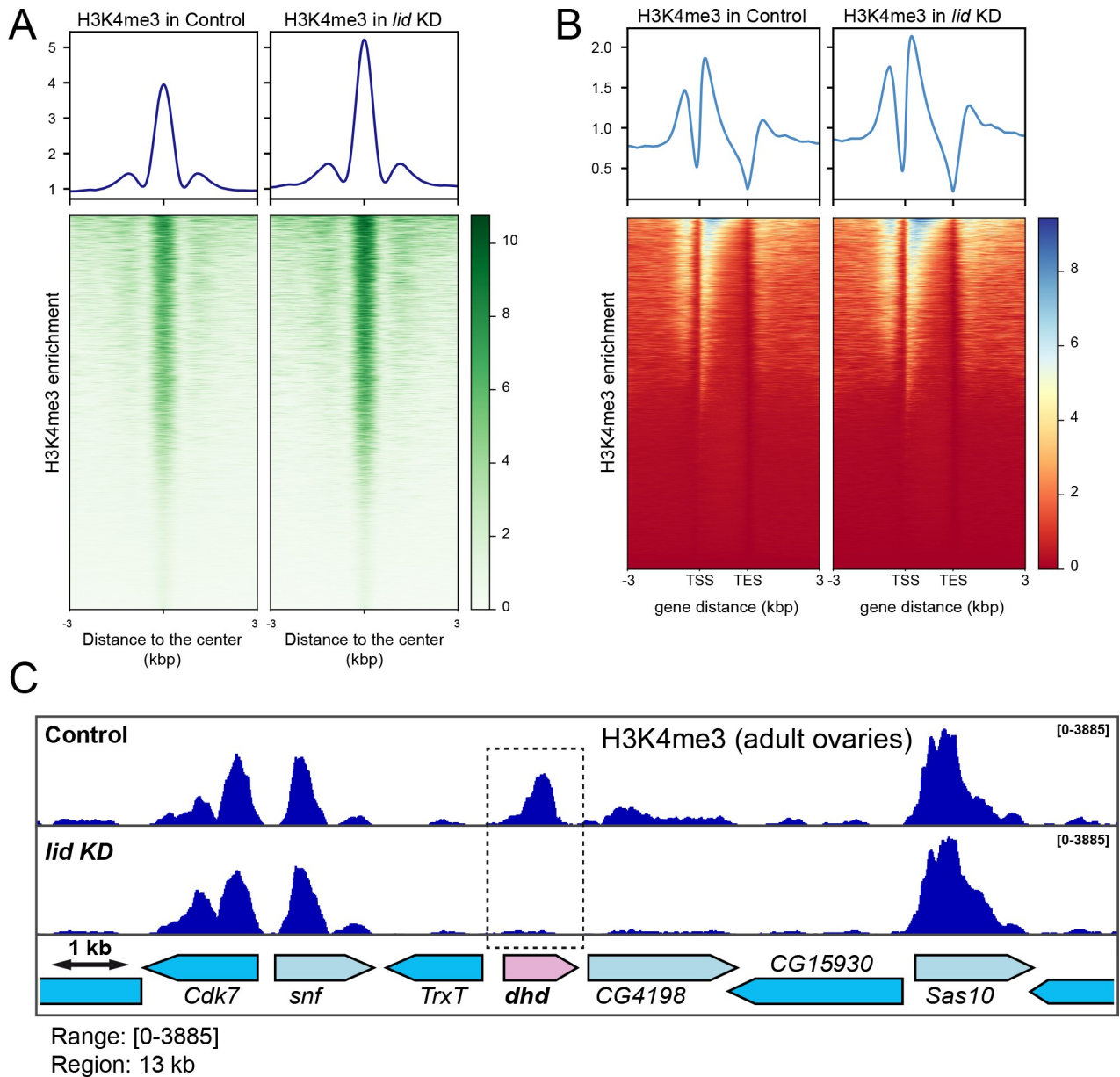


Fig 3. H3K4me3 ovarian ChIP-Seq analysis. A—H3K4me3 enrichment around peak center for Control and *lid* KD ovaries. Upper panels show the average profile around detected peak centers. Lower panels show read density heatmaps around the detected peak centers. B—H3K4me3 enrichment around gene loci for Control and *lid* KD ovaries. Upper panels show the average signal profile on genomic loci defined as 3kb upstream of annotated TSS to 3kb downstream of annotated TES. Lower panels show read density heatmaps around the same genomic loci. C—igv view of H3K4me3 occupancy on the *dhb* genomic region in Control and *lid* KD ovaries.

<https://doi.org/10.1371/journal.pgen.1008543.g003>

obvious candidate enhancer element in the vicinity of the *dhb* gene region, we cannot exclude this possibility.

Besides its JmjC demethylase domain, Lid/KDM5 possesses a conserved C-terminal PHD motif capable of binding H3K4me2/3. This binding motif is required for the recruitment of Lid at the promoter of target genes, where it could promote their activation [27]. The local recruitment of Lid, either through its C-terminal PHD motif or through its DNA binding ARID (AT-rich interaction domain) motif, or both, could thus establish a chromatin

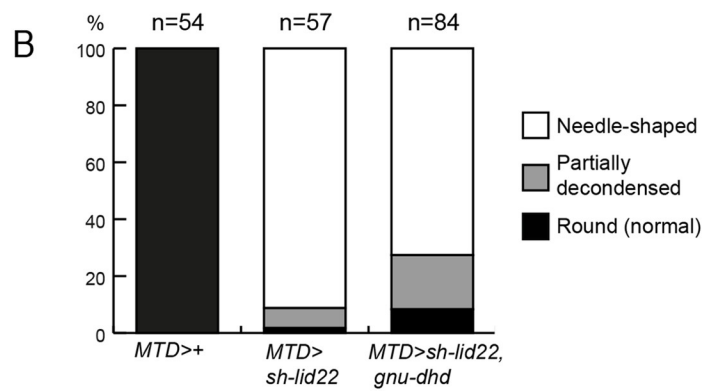
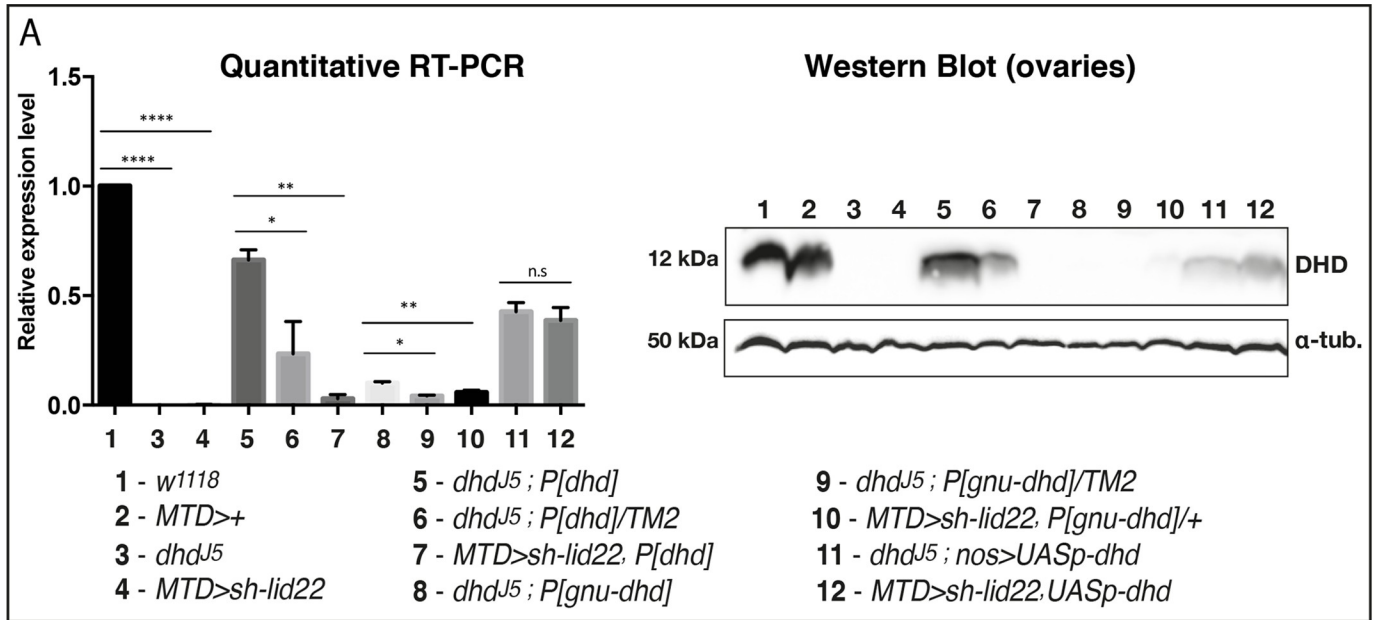
environment permissive to *dhd* massive expression in late oogenesis. In this context, the role of the Sin3A/HDAC1 complex also remains to be clarified. The Sin3A histone deacetylase complex is generally considered as a transcriptional repressor [15], but it also functions as a transcriptional activator in *Drosophila* S2 cells [17]. Lacking an intrinsic DNA binding ability [15], the recruitment of this complex to chromatin requires an additional factor. It is thus tempting to propose that Lid itself could recruit Sin3A/HDAC1 locally to activate *dhd* expression in female germ cells.

Forced *dhd* expression in *lid* KD ovaries partially restores sperm chromatin remodeling at fertilization

Taken together, our cytological and transcriptomic analyses strongly suggest that the loss of *dhd* expression in *lid* KD ovaries at least contributes to the observed fertilization phenotype. To directly test this possibility, we attempted to restore *dhd* expression in *lid* KD female germ cells through the use of transgenic constructs. A genomic transgene (P[*dhd*]) that fully rescued the fertility of *dhd* mutant females [6] only had a very limited impact on the hatching rate of *lid* KD embryos (Table 1) but quantitative RT-PCR analyses revealed that P[*dhd*] remained essentially silent in *lid* KD ovaries (Fig 4A). This result indicates that the 4.3 kb genomic region present in this transgene is sufficient to recapitulate the endogenous control exerted by Lid on *dhd* transcription. We then designed another transgene expressing *dhd* under the control of the *giant nuclei* (*gnu*) regulatory sequences. Like *dhd*, *gnu* is specifically expressed during oogenesis and is functionally required during zygote formation [35]. In addition, our RNA Seq data indicated that its expression is not controlled by Lid. We observed that the P[*gnu-dhd*] transgene indeed restored fertility to *dhd* homozygous mutant females albeit to modest level (about 7% embryo hatching rate; Table 1). In fact, rescued females only produced about 10% of the normal amount of *dhd* mRNA in their ovaries and the DHD protein remained almost undetectable in Western-blot (Fig 4A). Interestingly, when introduced into *lid* KD females, the P[*gnu-dhd*] transgene also slightly increased embryo hatching rate (Table 1). Furthermore, cytological examination of eggs laid by these females revealed a limited but clear improvement of sperm nuclear decondensation (Fig 4B and 4C). These results thus indicate that forced expression of *dhd* can improve the survival of *lid* KD eggs through its positive impact on sperm chromatin remodeling. Finally, we tried to further increase the level of expression of *dhd* by using a Gal4 inducible transgene, P[UAS-*dhd*^{WT}]. Indeed, induction of this transgene in the germline of *dhd*^{Δ5} mutant females fully restored their fertility (Table 1). We also observed a strong effect on the hatching rate of embryos laid by *lid* KD, P[UAS-*dhd*^{WT}] females (about 28%; Table 1). However, a P[UAS-*dhd*^{SXXXS}] transgene expressing a catalytic mutant DHD with no rescuing potential also improved the fertility of *lid* KD females. This effect suggests that Gal4 becomes limiting in the presence of two UAS transgenes, with a negative impact on knock-down efficiency. The fertility of P[UAS-*dhd*^{WT}] rescued females was nevertheless doubled compared to P[UAS-*dhd*^{SXXXS}] control females (Table 1), thus supporting the idea that partial *dhd* re-expression in *lid* KD ovaries significantly improved the probability of these eggs to form a viable, diploid zygote. Besides its already established roles in controlling the oocyte epigenome and the architecture of meiotic chromosomes, we show that the transcriptional regulation of *dhd* (and possibly additional early acting genes) is indeed a critical function of Lid and associated factors in female germ cells.

Trr controls sperm chromatin remodeling through a DHD-independent pathway

Intriguingly, germline KD of the Trithorax group protein Trithorax-related (Trr, also known as dMLL3/4), a histone methyltransferase responsible for monomethylation of H3K4 [36], was



C ♀ *MTD>sh-lid22, P[gnu-dhd]*

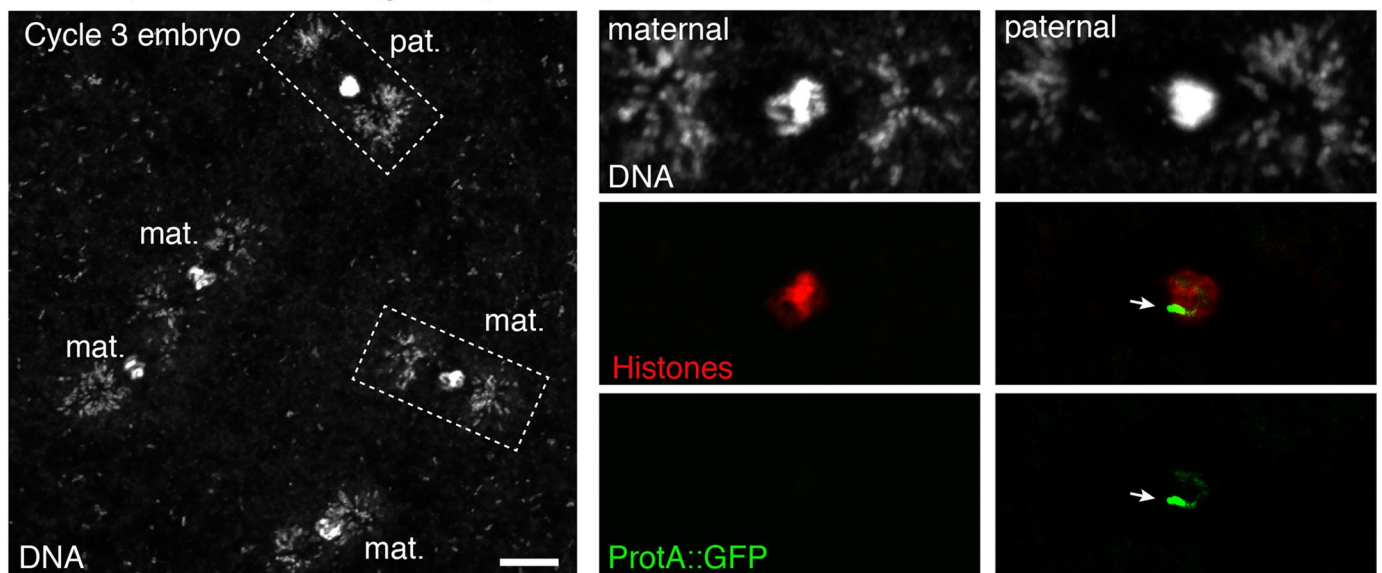


Fig 4. Forced expression of *dhd* partially rescues the *lid* KD phenotype. A—Left: RT-qPCR quantification of *dhd* mRNA levels in ovaries of indicated genotypes (normalized to *rp49* and relative to expression in *w¹¹¹⁸*). Data are presented as mean \pm SD of 2 biological replicates. P values indicate one-way ANOVA with Dunnett's multiple comparisons test to a control (**** P < 0.0001; ** P < 0.01, * P < 0.03; n.s = not significant). Right: Western blot analysis of DHD expression in ovaries of indicated genotypes. Alpha-tubulin detection is used as a loading control in Western-blotting. B—Quantification of sperm nuclear phenotype in eggs laid by females of indicated genotypes. C—Confocal images of a *MTD>lid22, P[gnu-dhd]* haploid embryo during the third nuclear division with incompletely remodeled male nucleus. Karyogamy has failed and the embryo contains four haploid nuclei of presumably maternal origin. The paternal nucleus (inset) still contains a region packaged with ProtA::GFP (arrow). Note that DNA positive dots at the spindle poles are *Wolbachia* endosymbionts. Scale bar: 10 μ m.

<https://doi.org/10.1371/journal.pgen.1008543.g004>

recently shown to induce a sperm decondensation defect at fertilization similar to the one reported here for *lid*, *Sin3a* and *rp3* KD [37]. In their study, however, Prudêncio *et al.* did not find any significant change in *dhd* mRNA level in *trr* KD early embryos. To more directly exclude any implication of DHD in the *trr* KD phenotypes, we stained control and KD eggs with an anti-DHD antibody. At fertilization, maternally-expressed DHD is abundant throughout the egg cytoplasm (100%, n = 41) but is rapidly degraded after pronuclear apposition. As expected, DHD protein remained undetectable in most *lid* KD eggs (92%, n = 50), including those that were fixed before the end of meiosis II (S8 Fig). In sharp contrast, DHD protein was normally detected in a majority of *trr* KD eggs, even though these eggs indeed contained a needle-shaped sperm nucleus still packaged with SNBPs (S8 Fig). This result thus confirms that Trr/dMLL3/4 controls sperm nuclear remodeling through a yet unknown, DHD-independent mechanism. Conversely, Trr was shown to control meiosis progression through the activation of *Idgf4* [37], a gene that is not affected by *lid* or *Sin3a* KD (this study). Thus Trr and Lid/Sin3A respectively activate a distinct repertoire of genes important for the oocyte-to-zygote transition and sperm chromatin remodeling.

Conclusion

Our maternal germline genetic screen has unveiled a complex and remarkably specific transcriptional regulation of the *dhd* gene by Lid/KDM5 and the Sin3A/HDAC1 complex. In addition to its crucial role in sperm protamine removal at fertilization, DHD was recently involved in the establishment of a redox state balance at the oocyte-to-zygote transition with a number of identified target proteins [7]. This important DHD-dependent thiol proteome remodeling is thus ultimately controlled by Lid and the SIN3 complex, underlying the critical contribution of these transcriptional regulators to this delicate developmental transition. Future work will aim at dissecting the chromatin mechanisms at play in setting up *dhd* specific activation in female germ cells.

Materials & methods

Drosophila strains

Flies were raised at 25°C on standard medium. The *w¹¹¹⁸* strain was used as a wild-type control. shRNAs lines used in this study (see S1 Table) were established by the Transgenic RNAi Project (TRiP) at Harvard Medical School and were obtained from the Bloomington Drosophila Stock Center at Indiana University. The *lid* and *Sin3A* shRNA lines target all predicted isoforms of their respective target genes. Additional stocks were *EGFP-Cid* [38], *P{otu-GAL4::VP16.R}1*; *P{GAL4-nos.NGT}40*; *P{GAL4::VP16-nos.UTR}MVD1* ("MTD-Gal4"), *P{GAL4::VP16-nos.UTR}MVD1* ("nos-Gal4"), *P[Mst35Ba-EGFP]* [24] and *Df(1)J5/FM7c* [39]. The *pUASP-dhd[WT]* and *pUASP-dhd[SXXS]* transgenic flies were a gift from C. Gonzalez and C. Molnar. The *PattB[gLid-WT-HA]* and *PattB[gLid-JMJC* -HA]* transgenic flies were kindly provided by P. Navarro-Costa [23].

Germline knock-down and fertility tests

To obtain *KD* females, virgin shRNA transgenic females were mass crossed with transgenic Gal4 males at 25°C and females of the desired genotype were recovered in the F1 progeny. To measure fertility, virgin females of different genotypes were aged for 2 days at 25°C in the presence of males and were then allowed to lay eggs on standard medium for 24 hours. Embryos were counted and then let to develop for at least 36 hours at 25°C. Unhatched embryos were counted to determine hatching rates.

Immunofluorescence and imaging

Early (0–30 min) and late (about 6 hours) embryos laid by randomly selected females were collected on agar plates. Embryos were dechorionated in bleach, fixed in a 1:1 heptane:methanol mixture and stored at -20°C. Embryos were washed three times (10 min each) with PBS1X 0.1%, Triton X-100 and were then incubated with primary antibodies in the same buffer on a wheel overnight at 4°C. They were then washed three times (20 min each) with PBS 0.1%, Triton X-100. Incubations with secondary antibodies were performed identically. Embryos were mounted in Dako mounting medium containing DAPI.

Ovaries were dissected in PBS-Triton 0.1% and fixed at room temperature in 4% formaldehyde in PBS for 25 minutes. Immunofluorescence was performed as for embryos except for secondary antibodies that were incubated four hours at room temperature. Ovaries were then mounted as described above.

Primary antibodies used were mouse monoclonal anti-histones (Sigma #MABE71; 1:1000), rabbit polyclonal anti-DHD (1:1000) [6], rat polyclonal anti-Lid (1:500) [14], mouse monoclonal anti-GFP (Roche #11814460001; 1:200) and Rat monoclonal anti alpha-tubulin (Abcam #ab6160; 1:50). Secondary antibodies were goat anti-rabbit antibodies (ThermoFisher Scientific, 1:500), goat anti-mouse or anti-rat antibodies (Jackson ImmunoResearch, 1:500) conjugated to AlexaFluor. Images were acquired on an LSM 800 confocal microscope (Carl Zeiss). Images were processed with Zen imaging software (Carl Zeiss) and Photoshop (Adobe).

Western blotting

Ovaries from 30 females were collected and homogenized in lysis buffer (20mM Hepes pH7.9, 100mM KCl, 0.1mM EDTA, 0.1mM EGTA, 5% Glycerol, 0.05% Igepal and protease inhibitors (Roche)). The protein extracts were cleared by centrifugation and stored at -80°C.

Eggs were collected every 30 min, dechorionated in bleach and quickly frozen in liquid nitrogen. Protein extracts were prepared from ca. 10 µl of embryos. Protein samples were run on 15% SDS polyacrylamide gel and transferred to Immun-Blot[®] PVDF membrane (Bio-Rad) for 1h at 60V. Membranes were blocked for 1h at room temperature in 5% non-fat milk in PBS 1X-Tween20 0.05%, followed by an overnight incubation with the primary antibody at 4°C in 5% non-fat milk in PBS1X-Tween20 0.05%. Secondary antibodies used were added and incubated for 2 hours at room temperature. Protein detection was performed using ECL solution according manufacturer's instruction (GE Healthcare). Antibodies used were: rabbit polyclonal anti-DHD (1/1000) [6], mouse monoclonal anti- α -Tubulin (Sigma Aldrich #T9026, 1:500), HRP-conjugated goat anti-mouse (Biorad #170–5047; 1:50 000) and peroxidase-conjugated goat anti-rabbit (Thermoscientific #32460; 1:20 000).

Gene expression analysis by RT-QPCR

Total RNA was extracted from ovaries of 3-day-old females using the NucleoSpin[®] RNA isolation kit (Macherey-Nagel), following the instructions of the manufacturer. Duplicates were

processed for each genotype. cDNAs were generated from 1µg of purified RNA with oligo (dT) primers using the SuperScriptTM II Reverse Transcriptase kit (Invitrogen).

Generated cDNAs were diluted to 1/5 and were used as template in a real time quantitative PCR assay using SYBR[®] Premix Ex TaqTM II (Tli RNaseH Plus) (Takara). All qRT-PCR reactions were performed in duplicate using Bio-Rad CFX-96 Connect system with the following conditions: 95°C for 1 min followed by 40 cycles of denaturation at 95°C for 10 s, annealing at 59°C for 30 s and extension at 72°C for 30 s. Relative fold change in gene expression was determined by the comparative quantification $\Delta\Delta CT$ method of analysis [40]. The housekeeping gene *rp49* was used to normalize cDNA amounts in the comparative analysis. The primer sets used in the PCR reactions were: *dhd*-forward 5'- TCTATGCGACATGGTGTGGT -3' and *dhd*-reverse 5'- TCCACATCGATCTTGAGCAC -3'; *lid*-forward 5'- ATTGGTTTCACGAGGATTGC -3' and *lid*-reverse 5'- CATAGCCACTTGGGTTCGATT -3'; *Rp49*-forward 5'- AAGATCGTGAAGAA GCGCAC -3' and *Rp49*-reverse 5'- GATACTGTCCCTTGAAGCGG -3'. Statistical tests were performed using GraphPad Prism version 6.00 for Mac OS X (GraphPad Software).

Ovarian RNA sequencing and analysis

For each samples, 8 pairs of ovaries were dissected from 6 day-old virgin females and total RNA were extracted using the NucleoSpin[®] RNA isolation kit (Macherey-Nagel), following the instructions of the manufacturer. Extracted RNAs were treated with TurboTMDNase (Ambion #AM2238). After DNase inactivation, RNAs were purified using the NucleoSpin[®] RNA Clean-up XS kit (Macherey-Nagel) according to manufacturer's instructions. Sequencing was completed on two biological replicates of each genotype:

Control KD (*MTD-Gal4>+*)

$P\{w[+mC] = otu-GAL4::VP16.R\}1, w[*]/y[1] v[1]; P\{w[+mC] = GAL4-nos.NGT\}40/+; P\{w[+mC] = GAL4::VP16-nos.UTR\}CG6325[MVD1]/P\{y[+t7.7] = CaryP\}attP2$

lid KD (*MTD-Gal4>shRNA lid*)

$P\{w[+mC] = otu-GAL4::VP16.R\}1, w[*]/y[1] sc[*] v[1]; P\{w[+mC] = GAL4-nos.NGT\}40/+; P\{w[+mC] = GAL4::VP16-nos.UTR\}CG6325[MVD1]/P\{y[+t7.7] v[+t1.8] = TRiP.GLV21071\} attP2$

Sin3A KD (*MTD-Gal4>shRNA Sin3A*)

$P\{w[+mC] = otu-GAL4::VP16.R\}1, w[*]/y[1] sc[*] v[1]; P\{w[+mC] = GAL4-nos.NGT\}40/+; P\{w[+mC] = GAL4::VP16-nos.UTR\}CG6325[MVD1]/P\{y[+t7.7] v[+t1.8] = TRiP.HMS00359\}attP2$

Sequencing libraries for each sample were synthesized using TruSeq Stranded mRNA kit (Illumina) following supplier recommendations (Sample Preparation Guide—PN 15031047, version Rev.E Oct 2013) and were sequenced on Illumina HiSeq 4000 sequencer as Single-Reads 50 base reads following Illumina's instructions (GenomEast platform, IGBM, Strasbourg, France). Image analysis and base calling were performed using RTA 2.7.3 and bcl2fastq 2.17.1.14. Adapter dimer reads were removed using DimerRemover. Sequenced reads were mapped to the *Drosophila melanogaster* genome assembly dm6 using TopHat (version 2.1.1) with default option. The aligned reads were assigned to genes by FeatureCounts, run with default options on the dmel-all-r6.15 version of the *Drosophila melanogaster* genome annotation. Differentially expressed genes were identified using the R-package DESeq2 (version 1.14.1). The annotated genes exhibiting an adjusted-P < 0.001 were considered differentially expressed compared to Control.

Chromatin immunoprecipitation, sequencing and analysis

ChIP assays were performed as previously described [41]. Two biological replicates for *control* KD and *lid* KD ovaries (same genotypes as for RNA Seq) were processed and analyzed. For

each biological replicate, eighty ovary pairs were dissected from 2 day-old females and flash frozen. Dissected ovaries were fixed in 1.8% formaldehyde at room temperature for 10 minutes. Chromatin was sonicated using a Diagenod Bioruptor (18 cycles, high intensity, 30s on/30s off) to generate random DNA fragments from 100 to 800 base pairs. Sheared chromatin was incubated overnight at 4 °C with H3K4me3 antibody (ab8580 Abcam). Immunoprecipitated samples were treated with RNase A, proteinase K and DNA purified using the ChIP DNA Purification kit (Active Motif #58002) following the manufacturer's instructions. Quantification assessment of purified DNA was done using Qbit dsDNA HS Assay on the Qbit fluorometer (Invitrogen). Immunoprecipitated DNA quality was evaluated on a Bioanalyzer 2100 (Agilent).

Sequencing libraries for each sample were synthesized using Diagenode MicroPlex Library Preparation kit according to supplier recommendations (version 2.02.15) and were sequenced on Illumina HiSeq 4000 sequencer as Paired-End 50 base reads following Illumina's instructions (GenomEast platform, IGBM, Strasbourg, France). Image analysis and base calling were performed using RTA 2.7.3 and bcl2fastq 2.17.1.14. Adapter dimer reads were removed using DimerRemover. Sequenced reads were mapped to the *Drosophila melanogaster* genome assembly dm6 using Bowtie (version 2.3.3) with default option. Only uniquely aligned reads have been retained for further analyses. Duplicated reads were removed using picard-tools (version 2.17.10). Peak calling was performed for each individual samples and on merged biological replicates using MACS algorithm (version 2.1.1) with default option and a relaxed q-value cut-off of 0.1. Consistent peaks between biological replicates were identified using irreproducible discovery rate (IDR version 2.0.3) with a 0.05 cut-off. Differentially modified H3K4me3 peaks between Control and *lid* Knock-down ovaries were identified using the R-package DiffBind (version 2.2.12) with a 0.05 FDR cut-off.

Data visualization

The Deeptools software was used to convert alignment files to bigwig (bamCoverage) and to generate H3K4me3 heatmap and density profiles (computeMatrix and plotHeatmap). The generated bigwig files were visualized using IGV software.

Supporting information

S1 Fig. Developmental defects of *lid* KD embryos. Embryos were collected for four hours and aged for another four hours at 25 °C before DAPI staining and examination in fluorescent microscopy. More than 85% of *lid* KD embryos arrest development before the blastoderm stage. In contrast, 100% of control embryos had reached gastrula or later stages. (TIF)

S2 Fig. Meiosis II is not visibly affected in eggs from *lid* KD females. A—Representative confocal images of eggs in metaphase of meiosis II stained for DNA (blue), alpha-tubulin (red) and ProtA::GFP (green). The tandem of meiotic spindles is shown on the left, the corresponding male nucleus from the same egg is on the right. Bars: 5 μm. B—Quantification of meiosis II phenotypes (normal or abnormal chromosome segregation). (TIF)

S3 Fig. Phenotype of *Sin3A* KD and *rpD3* KD eggs/embryos. A—Confocal images of *Sin3A* KD eggs stained for DNA at the indicated stages. The sperm nucleus in the left panel is indicated (arrow). Bar: 10 μm. PB: Polar bodies. B—Confocal images of *rpD3* KD early embryos (from ProtA::GFP fathers) stained for DNA and anti-GFP. The sperm nucleus is indicated

(arrows). Bar: 10 μ m. PB: Polar bodies.
(TIF)

S4 Fig. Lid is not directly involved in sperm chromatin remodeling at fertilization. A—Top row: confocal images of stage 10 egg chambers from control (left) and lid KD (right) females stained for DNA (red) and anti-Lid (green). Middle row: detail of a nurse cell nucleus. Bottom row: detail of the oocyte germinal vesicle (oocyte nucleus). Bar: 20 μ m. B—Confocal images of the male pronucleus and the female pronucleus from a control egg in meiosis II stained for DNA and anti-Lid. Bar: 10 μ m. Quantification of Lid positive nuclei is indicated. C—Confocal images of a control (left) and lid KD (right) blastoderm embryo with same staining as in B. Bar: 10 μ m. Quantifications of embryos with a positive/negative nuclear Lid staining are indicated for each genotype.

(JPG)

S5 Fig. Lid and Sin3A control *dhd* expression in female germ cells. A—Principal Component Analysis of Control, *lid* KD and *Sin3A* KD ovarian transcriptomes (two biological replicates for each genotype). B—Volcano plot representations of Differentially-Expressed genes in Control vs *lid* KD (left) and Control vs *Sin3A* KD (right). C—RT-qPCR quantification of *dhd* mRNA levels in ovaries of indicated genotypes. mRNA levels were normalized to rp49 and shown as relative expression in MTD>+ control. Error bars represent SD (Dunnett's multiple comparisons test to the control MTD>+, **** P < 0.0001). D—Western blot analysis of DHD in adult ovaries (left) and 0-30min postfertilization embryos (right). α -tubulin was used as a loading control. E—Western blot analysis of DHD in adult ovaries of indicated genotypes. α -tubulin was used as a loading control.

(TIF)

S6 Fig. Top twelve most downregulated and upregulated genes in *lid* KD and *Sin3A* KD transcriptomes.

(TIF)

S7 Fig. The JmjC domain of Lid is required for normal *dhd* expression. A—Embryo hatching rates from females of indicated genotypes. B—RT-qPCR quantification of *dhd* (left) and *lid* (right) mRNA levels in ovaries of indicated genotypes. mRNA levels were normalized to rp49 and shown as relative expression in *w¹¹¹⁸* control. Error bars represent SD (Dunnett's multiple comparisons test to the control (** P < 0.01; *** P = 0.0002). C—Analysis of paternal GFP::Cid expression in late embryos from indicated females (as in Fig 1B).

(TIF)

S8 Fig. *trr* KD does not affect *dhd* expression. A—Confocal images of representative embryos of the indicated genotypes stained for DNA and anti-DHD. The fertilizing sperm nucleus is magnified in insets. Bar: 20 μ m. B—Details of maternal chromosomes (top row) and sperm nucleus (bottom row) from a representative *trr* KD egg stained for ProtA::GFP and histones.

(JPG)

S1 Table. Haploid TRiP genetic screen.

(XLSX)

S2 Table. Differentially expressed genes in *lid* KD and *Sin3A* KD ovaries.

(XLSX)

S3 Table. Quantitative analysis of H3K4me3 differential enrichment in Control vs *lid* KD ovarian ChIP-Seq.

(XLSX)

Acknowledgments

We thank Ferran Azorin, Cayetano Gonzalez, Cristina Molnar and Paulo Navarro-Costa for sharing fly stocks and antibodies. We are grateful to the TRiP projects and Bloomington *Drosophila* Stock Center for shRNA stocks. The authors would like to thank the members of the IGBMC GenomEast platform for their help. We also thank Raphaëlle Dubruille for her helpful comments on the manuscript.

Author Contributions

Conceptualization: Daniela Torres-Campana, Shuhei Kimura, Guillermo A. Orsi, Benjamin Loppin.

Data curation: Guillermo A. Orsi, Gérard Benoit.

Formal analysis: Gérard Benoit.

Funding acquisition: Benjamin Loppin.

Investigation: Daniela Torres-Campana, Shuhei Kimura, Béatrice Horard, Benjamin Loppin.

Methodology: Gérard Benoit.

Supervision: Béatrice Horard, Benjamin Loppin.

Validation: Daniela Torres-Campana, Guillermo A. Orsi, Béatrice Horard, Gérard Benoit, Benjamin Loppin.

Writing – original draft: Benjamin Loppin.

Writing – review & editing: Daniela Torres-Campana, Guillermo A. Orsi, Béatrice Horard, Gérard Benoit, Benjamin Loppin.

References

1. Loppin B, Dubruille R, Horard B (2015) The intimate genetics of *Drosophila* fertilization. *Open Biol* 5: 150076. <https://doi.org/10.1098/rsob.150076> PMID: 26246493
2. Hamm DC, Harrison MM (2018) Regulatory principles governing the maternal-to-zygotic transition: insights from *Drosophila melanogaster*. *Open Biol* 8: 180183. <https://doi.org/10.1098/rsob.180183> PMID: 30977698
3. Spradling AC (1993) Developmental genetics of oogenesis. *The Development of Drosophila melanogaster*—Cold Spring Harbor Laboratory Press. 1–69.
4. Eirin-López JM, Ausió J (2009) Origin and evolution of chromosomal sperm proteins. *Bioessays* 31: 1062–1070. <https://doi.org/10.1002/bies.200900050> PMID: 19708021
5. Rathke C, Baarends WM, Awe S, Renkawitz-Pohl R (2014) Chromatin dynamics during spermiogenesis. *Biochim Biophys Acta*. 1839: 155–168. <https://doi.org/10.1016/j.bbaggm.2013.08.004> PMID: 24091090
6. Tirmarche S, Kimura S, Dubruille R, Horard B, Loppin B (2016) Unlocking sperm chromatin at fertilization requires a dedicated egg thioredoxin in *Drosophila*. *Nature Commun* 7: 13539. <https://doi.org/10.1038/ncomms13539>
7. Petrova B, Liu K, Tian C, Kitaoka M, Freinkman E, Yang J, et al. (2018) Dynamic redox balance directs the oocyte-to-embryo transition via developmentally controlled reactive cysteine changes. *Proc Natl Acad Sci USA* 115: E7978–E7986. <https://doi.org/10.1073/pnas.1807918115> PMID: 30082411
8. Horard B, Sapey-Triomphe L, Bonnefoy E, Loppin B (2018) ASF1 is required to load histones on the HIRA complex in preparation of paternal chromatin assembly at fertilization. *Epigenetics Chromatin* 11: 19. <https://doi.org/10.1186/s13072-018-0189-x> PMID: 29751847
9. Ni J-Q, Zhou R, Czech B, Liu L-P, Holderbaum L, Yang-Zhou D, et al. (2011) A genome-scale shRNA resource for transgenic RNAi in *Drosophila*. *Nat Meth* 8: 405–407. <https://doi.org/10.1038/nmeth.1592>
10. Delabaere L, Orsi GA, Sapey-Triomphe L, Horard B, Couble P, Loppin B (2014) The Spartan Ortholog Maternal Haploid Is Required for Paternal Chromosome Integrity in the *Drosophila* Zygote. *Curr Biol* 24: 2281–2287. <https://doi.org/10.1016/j.cub.2014.08.010> PMID: 25242033

11. Gildea JJ, Lopez R, Shearn A (2000) A screen for new trithorax group genes identified little imaginal discs, the *Drosophila melanogaster* homologue of human retinoblastoma binding protein 2. *Genetics* 156: 645–663. PMID: [11014813](https://pubmed.ncbi.nlm.nih.gov/11014813/)
12. Secombe J, Li L, Carlos L, Eisenman RN (2007) The Trithorax group protein Lid is a trimethyl histone H3K4 demethylase required for dMyc-induced cell growth. *Genes & Dev* 21: 537–551. <https://doi.org/10.1101/gad.1523007>
13. Lloret-Llinares M, Carr CM, Vaquero A, de Olano N, Azorin F (2008) Characterization of *Drosophila melanogaster* JmjC+N histone demethylases. *Nucleic Acids Res*. 36: 2852–2863. <https://doi.org/10.1093/nar/gkn098> PMID: [18375980](https://pubmed.ncbi.nlm.nih.gov/18375980/)
14. Lloret-Llinares M, Perez-Lluch S, Rossell D, Moran T, Ponsa-Cobas J, Auer H, et al. (2012) dKDM5/LID regulates H3K4me3 dynamics at the transcription-start site (TSS) of actively transcribed developmental genes. *Nucleic Acids Res*. 40: 9493–9505. <https://doi.org/10.1093/nar/gks773> PMID: [22904080](https://pubmed.ncbi.nlm.nih.gov/22904080/)
15. Grzenda A, Lomberk G, Zhang J-S, Urrutia R (2009) Sin3: Master scaffold and transcriptional corepressor. *Biochim Biophys Acta* 1789: 443–450. <https://doi.org/10.1016/j.bbagra.2009.05.007> PMID: [19505602](https://pubmed.ncbi.nlm.nih.gov/19505602/)
16. Spain MM, Caruso JA, Swaminathan A, Pile LA (2010) *Drosophila* SIN3 Isoforms Interact with Distinct Proteins and Have Unique Biological Functions. *J Biol Chem* 285: 27457–27467. <https://doi.org/10.1074/jbc.M110.130245> PMID: [20566628](https://pubmed.ncbi.nlm.nih.gov/20566628/)
17. Gajan A, Barnes VL, Liu M, Saha N, Pile LA (2016) The histone demethylase dKDM5/LID interacts with the SIN3 histone deacetylase complex and shares functional similarities with SIN3. *Epigenetics Chromatin* 9:4 <https://doi.org/10.1186/s13072-016-0053-9> PMID: [26848313](https://pubmed.ncbi.nlm.nih.gov/26848313/)
18. Liu M, Pile LA (2017) The Transcriptional Corepressor SIN3 Directly Regulates Genes Involved in Methionine Catabolism and Affects Histone Methylation, Linking Epigenetics and Metabolism. *J Biol Chem* 292: 1970–1976. <https://doi.org/10.1074/jbc.M116.749754> PMID: [28028175](https://pubmed.ncbi.nlm.nih.gov/28028175/)
19. Barnes VL, Bhat A, Unnikrishnan A, Heydari AR, Arking R, Pile LA (2014) SIN3 is critical for stress resistance and modulates adult lifespan. *Aging* 6: 645–660. <https://doi.org/10.18632/aging.100684> PMID: [25133314](https://pubmed.ncbi.nlm.nih.gov/25133314/)
20. Moshkin YM, Kan TW, Goodfellow H, Bezstarosti K, Maeda RK, Pilyugin M, et al. (2009) Histone Chaperones ASF1 and NAP1 Differentially Modulate Removal of Active Histone Marks by LID-RPD3 Complexes during NOTCH Silencing. *Mol Cell* 35: 782–793. <https://doi.org/10.1016/j.molcel.2009.07.020> PMID: [19782028](https://pubmed.ncbi.nlm.nih.gov/19782028/)
21. Lee N, Erdjument-Bromage H, Tempst P, Jones RS, Zhang Y (2009) The H3K4 Demethylase Lid Associates with and Inhibits Histone Deacetylase Rpd3. *Mol Cell Biol* 29: 1401–1410. <https://doi.org/10.1128/MCB.01643-08> PMID: [19114561](https://pubmed.ncbi.nlm.nih.gov/19114561/)
22. Kronja I, Yuan B, Eichhorn SW, Dzeyk K, Krijgsveld J, Bartel DP, et al. (2014) Widespread Changes in the Posttranscriptional Landscape at the *Drosophila* Oocyte-to-Embryo Transition. *Cell Reports* 7: 1495–1508. <https://doi.org/10.1016/j.celrep.2014.05.002> PMID: [24882012](https://pubmed.ncbi.nlm.nih.gov/24882012/)
23. Navarro-Costa P, McCarthy A, Prudêncio P, Greer C, Guilgur LG, Becker JORD, et al. (2016) Early programming of the oocyte epigenome temporally controls late prophase I transcription and chromatin remodelling. *Nature Commun* 7: 1–15. <https://doi.org/10.1038/ncomms12331>
24. Manier MK, Belote JM, Berben KS, Novikov D, Stuart WT, Pitnick S (2010) Resolving Mechanisms of Competitive Fertilization Success in *Drosophila melanogaster*. *Science* 328: 354–357. <https://doi.org/10.1126/science.1187096> PMID: [20299550](https://pubmed.ncbi.nlm.nih.gov/20299550/)
25. Zhaunova L, Ohkura H, Breuer M (2016) Kdm5/Lid Regulates Chromosome Architecture in Meiotic Prophase I Independently of Its Histone Demethylase Activity. *PLoS Genet*. 12: e1006241. <https://doi.org/10.1371/journal.pgen.1006241> PMID: [27494704](https://pubmed.ncbi.nlm.nih.gov/27494704/)
26. Drelon C, Belalcazar HM, Secombe J. The Histone Demethylase KDM5 Is Essential for Larval Growth in *Drosophila* (2018) *Genetics* 209: 773–787. <https://doi.org/10.1534/genetics.118.301004> PMID: [29764901](https://pubmed.ncbi.nlm.nih.gov/29764901/)
27. Liu X, Secombe J (2015) The Histone Demethylase KDM5 Activates Gene Expression by Recognizing Chromatin Context through Its PHD Reader Motif. *Cell Reports* 13: 2219–2231. <https://doi.org/10.1016/j.celrep.2015.11.007> PMID: [26673323](https://pubmed.ncbi.nlm.nih.gov/26673323/)
28. Emelyanov AV, Fyodorov DV (2016) Thioredoxin-dependent disulfide bond reduction is required for protamine eviction from sperm chromatin. *Genes & Dev* 30: 2651–2656. <https://doi.org/10.1101/gad.290916.116>
29. Sandler JE, Stathopoulos A (2016) Quantitative Single-Embryo Profile of *Drosophila* Genome Activation and the Dorsal-Ventral Patterning Network. *Genetics* 202: 1575–1584. <https://doi.org/10.1534/genetics.116.186783> PMID: [26896327](https://pubmed.ncbi.nlm.nih.gov/26896327/)

30. Zamurrad S, Hatch HAM, Drelon C, Belalcazar HM, Secombe J (2018) A *Drosophila* Model of Intellectual Disability Caused by Mutations in the Histone Demethylase KDM5. *Cell Reports* 22: 2359–2369. <https://doi.org/10.1016/j.celrep.2018.02.018> PMID: 29490272
31. Li L, Greer C, Eisenman RN, Secombe J (2010) Essential functions of the histone demethylase lid. *PLoS Genet.* 6: e1001221. <https://doi.org/10.1371/journal.pgen.1001221> PMID: 21124823
32. Lussi YC, Mariani L, Friis C, Peltonen J, Myers TR, Krag C, et al. (2016) Impaired removal of H3K4 methylation affects cell fate determination and gene transcription. *Development* 143: 3751–3762. <https://doi.org/10.1242/dev.139139> PMID: 27578789
33. Kidder BL, Hu G, Zhao K (2014) KDM5B focuses H3K4 methylation near promoters and enhancers during embryonic stem cell self-renewal and differentiation. *Genome Biol* 15: R32. <https://doi.org/10.1186/gb-2014-15-2-r32> PMID: 24495580
34. Outchkourov NS, Muiño JM, Kaufmann K, van IJcken WFJ, Koerkamp MJG, van Leenen D, et al. (2013) Balancing of Histone H3K4 Methylation States by the Kdm5c/SMCX Histone Demethylase Modulates Promoter and Enhancer Function. *Cell Reports* 3: 1071–1079. <https://doi.org/10.1016/j.celrep.2013.02.030> PMID: 23545502
35. Freeman M, Nüsslein-Volhard C, Glover DM (1986) The dissociation of nuclear and centrosomal division in *gnu*, a mutation causing giant nuclei in *Drosophila*. *Cell* 46: 457–468. [https://doi.org/10.1016/0092-8674\(86\)90666-5](https://doi.org/10.1016/0092-8674(86)90666-5) PMID: 3089628
36. Herz HM, Mohan M, Garruss AS, Liang K, Takahashi YH, Mickey K, et al. (2012) Enhancer-associated H3K4 monomethylation by Trithorax-related, the *Drosophila* homolog of mammalian Mll3/Mll4. *Genes & Dev* 26: 2604–2620. <https://doi.org/10.1101/gad.201327.112>
37. Prudêncio P, Guilgur LG, Sobral J, Becker JD, Martinho RG, Navarro-Costa P (2018) The Trithorax group protein dMLL3/4 instructs the assembly of the zygotic genome at fertilization. *EMBO Rep* 19: e45728. <https://doi.org/10.15252/embr.201845728> PMID: 30037897
38. Schuh M, Lehner CF, Heidmann S (2007) Incorporation of *Drosophila* CID/CENP-A and CENP-C into centromeres during early embryonic anaphase. *Curr Biol* 17: 237–243. <https://doi.org/10.1016/j.cub.2006.11.051> PMID: 17222555
39. Salz HK, Flickinger TW, Mittendorf E, Pellicena-Palle A, Petschek JP, Brown Albretch E (1994) The *Drosophila* Maternal Effect Locus deadhead Encodes a Thioredoxin Homolog Required for Female Meiosis and Early Embryonic Development. *Genetics* 136: 1075–1086. PMID: 7516301
40. Livak KJ, Schmittgen TD (2001) Analysis of Relative Gene Expression Data Using Real-Time Quantitative PCR and the 2⁻ $\Delta\Delta$ CT Method. *Methods* 25: 402–408. <https://doi.org/10.1006/meth.2001.1262> PMID: 11846609
41. Grentzinger T, Armenise C, Brun C, Mugat B, Serrano V, Pelisson A, et al. (2012) piRNA-mediated transgenerational inheritance of an acquired trait. *Genome Res* 22: 1877–1888. <https://doi.org/10.1101/gr.136614.111> PMID: 22555593